Characterization of the Complex Permittivity of Brain Tissues up to 50 GHz Utilizing a Two-Port Microstrip Test Fixture

Mohammad-Reza Tofighi, *Member, IEEE,* and Afshin S. Daryoush, *Fellow, IEEE*

***Abstract*—Broad-band complex-permittivity values of biological tissues above 20 GHz obtained from direct measurements have not been reported in the literature. This paper presents for the first time the measurement results of complex permittivity of brain grey and white matters from 15 to 50 GHz utilizing a two-port microstrip test fixture. Test fixture S-parameters are simulated employing the finite-element method. To apply the data obtained from the simulation in complex-permittivity extraction, an efficient procedure, using the linear least square technique, is introduced to fit the modeling results to a rational function of complex permittivity, which is similar to the transfer function for a linear system. This fitting procedure is computationally more efficient than the previously developed fitting methods. Measurements are performed on slices of brain sample using a calibrated network analyzer utilizing custom designed through-reflect-line (TRL) calibration standards. The measurements are corrected for the residual errors observed in the measurement results due to the lack of performance repeatability of coaxial-to-microstrip launchers utilized in the TRL calibration standards. Finally, the measured results for brain matters are fitted to a single term Cole–Cole relation representing the dispersion characteristics of white and grey matters up to 50 GHz.**

***Index Terms*—Biological tissue, complex-permittivity measurement, millimeter wave, test fixture, TRL calibration.**

I. Introduction

In RECENT years, there has been a lot of interest in understanding and quantification of electromagnetic fields interaction with biological systems and their medical applications [1]. Some of this interest stems from therapeutic applications of microwaves [2] and, more recently, the potential health hazards due to the advent of wireless communications [3]. As the demand for higher mobility and information capacity drives implementation of communication services at higher microwave and millimeter-wave frequencies, interests grow in medical applications over these frequency ranges [4].

Both the therapeutic applications [2] and dosimetery [3] require knowledge of the dielectric property of the tissues. Most comprehensive reviews of the available dielectric properties of biological tissues [5] are limited up to 20 GHz and, with the exception of blood complex-permittivity data [6], there are only scattered tissue data in the millimeter-wave frequency range. Complex-permittivity measurement of lossy and biological materials is well established below 20 GHz [7] using an open-ended coaxial probe in contact with the tissue under test (TUT).

Manuscript received May 3, 2001; revised December 12, 2001.

The authors are with the Department of Electrical and Computer Engineering, Drexel University, Philadelphia, PA 19104 USA (e-mail: mtofighi@ece.drexel.edu; daryoush@ece.drexel.edu).

Digital Object Identifier 10.1109/TMTT.2002.803432.

With the advent of the automatic network analyzer (ANA), accurate two-port measurements up to millimeter-wave frequencies can be accomplished. We have already reported primary features of an alternative approach for complex-permittivity measurement of biological materials based on a two-port microstrip test fixture proposed for measurements up to millimeter-wave frequencies [8], [9].

The technique is unique due to a few important features. Employing the two-port measurement is motivated by the availability of a powerful two-port calibration, i.e., through-reflect-line (TRL) [10], and existence of a higher sensitivity of S_{21} compared to S_{11} with respect to any change in permittivity of the TUT [8], [9].

Moreover, the sensitivity and range of operation of the test fixture can be controlled through changing the critical dimensions of the test fixture; whereas the traditional coaxial type probes do not easily lend themselves to dimensional variability. A slotted waveguide section has also been used for tissue measurement at lower frequencies [11]. However, our test fixture is based on a microstrip transmission line, which has a broader bandwidth over millimeter-wave waveguide structures [6]. To the best of our knowledge, there is no published tissue permittivity values utilizing planar type structures (i.e., microstrip line, coplanar waveguide, etc.) even though they have already been reported for characterization of other materials [12].

This paper presents realization of this proposed technique and its application to complex-permittivity measurement of white and grey brain tissues up to 50 GHz for the first time. The test-fixture setup is presented in Section II, where a commercial finite-element method (FEM) package from Agilent (HFSS 5.2) is used for full-wave characterization of the test fixture. The model is used to evaluate the performance of the test fixture in terms of its S-parameters when the TUT is embedded in it. A set of data is obtained for the parametric solution of the test fixture for different permittivity values and is fitted to a rational function, which is similar to the pole-zero expansion of the transfer function for a linear system. The fitting procedure utilizes a linear least square algorithm and yields a set of parameters to represent the complex S-parameters as a function of complex permittivity at each measurement frequency. The procedure not only provides good accuracy, but is computationally much more efficient compared to a previously reported fitting technique, which is based on a nonlinear least square method [13]. To solve the inverse solution of this problem, an extraction method is presented in Section III for determining the complex permittivity of the TUT.

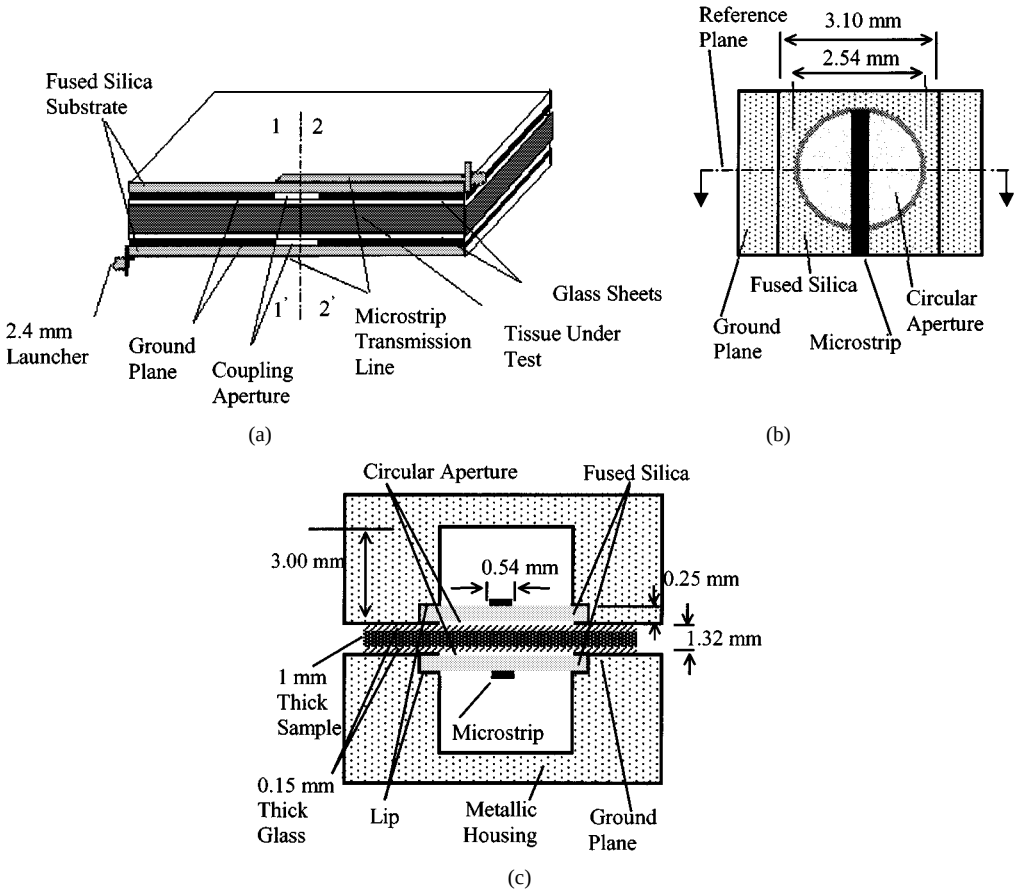

Fig. 1. (a) Longitudinal-section view of the microstrip test fixture, where the two microstrip lines are coupled through two apertures, glass sheets, and the tissue. Microstrip coupling structure for up to 50 GHz measurement. (b) Top view. (c) Front view.

A comparison of the measurement and simulation results is presented in Section IV, where the complex permittivity of water and white and grey brain matters at 27 °C are extracted for a frequency range of 15–50 GHz. Moreover, the measured complex-permittivity values of brain white and grey matters are corrected for the residual errors due to the lack of repeatability of the coaxial-to-microstrip launchers. These new measurement results are fitted to a Cole–Cole model for γ dispersion [14]. Finally, an error analysis for the extracted results is also performed.

II. Test Fixture

A. Test-Fixture Structure

Fig. 1(a) shows the conceptual drawing of the two-port test fixture. Open-circuited microstrip transmission lines are coupled to the TUT through two small apertures. The sample is sandwiched between glass plates and then inserted between the microstrip ground planes. Planes 1–1′ and 2–2′ are the reference planes where the effects of embedding networks are removed. Microstrip lines and apertures are etched over the two sides of a fused silica substrate ($\varepsilon_r = 4.1$). Two coaxial-to-microstrip-line launchers provide transitions from the network analyzer test-set cables to the fixture.

A 100-mil (i.e., 2.54 mm)-diameter circular aperture is considered [see Fig. 1(b)] [8], [9] as a compromise between the coupling factor and spatial resolution. To have a realizable

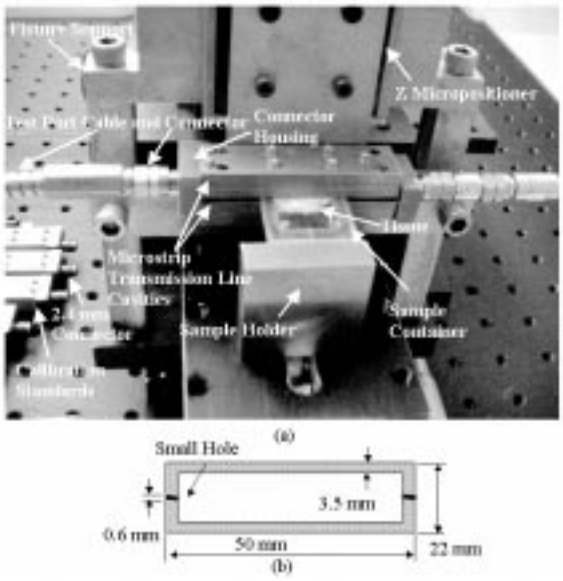

Fig. 2. (a) Close look at the test-fixture cavities, input launchers, and sample placement. (b) Sample container structure made from an acrylic sheet (1.02-mm thick).

microstrip-line test fixture with the aperture on the ground plane facing the sample, the width of the fused silica substrate should be slightly more than the width of air-filled space above. The substrate sits inside lips provided in the enclosure. Therefore, the microstrip cross section is not a complete

TABLE I
FUNCTIONS USED TO FIT THE DATA OBTAINED FROM MODELING AND DEFINITIONS OF THE RELATED PARAMETERS

	Along f and ε Spaces	Along f Space	Along ε Space
Fitting Function	$S_{ij}=\dfrac{\sum_{n=0}^{N}\sum_{p=0}^{P}\alpha_{np}\zeta^{p}(j\omega)^{n}}{1+\sum_{m=1}^{M}\sum_{q=1}^{Q}\beta_{mq}\zeta^{q}(j\omega)^{m}}$ Eq. (1)	$S_{ij}=\dfrac{\sum_{n=0}^{N}a_{n}(j\omega)^{n}}{1+\sum_{m=1}^{M}b_{m}(j\omega)^{m}}$ Eq. (2)	$S_{ij}=\dfrac{\sum_{p=0}^{P}A_{p}\zeta^{p}}{1+\sum_{q=1}^{Q}B_{q}\zeta^{q}}$ Eq. (4)
Parameters	α_{np} β_{mq}	$a_{n}=\sum_{p=0}^{P}\alpha_{np}\zeta^{p}$ $b_{m}=\sum_{q=1}^{Q}\beta_{mq}\zeta^{q}$ Eq. (3)	$A_{p}=\sum_{n=0}^{N}\alpha_{np}(j\omega)^{p}$ $B_{q}=\sum_{m=1}^{M}\beta_{mq}(j\omega)^{q}$ Eq. (5)

rectangle [see Fig. 1(c)]. The characteristic impedance of the line is also close to 50 Ω to guarantee a low return loss for the coaxial-to-microstrip launcher. Selected microstrip dimensions provide a single mode operation up to 53.5 GHz with the second-order mode having 37-dB/cm attenuation at 50 GHz.

B. Test-Fixture Setup

Fig. 2(a) presents a close look of the test-fixture microstrip cavity structures, ANA test port cables and connectors, input launchers, and TUT embedded in the test fixture. The TUT is placed between two microstrip cavities, as shown in Fig. 2(a). This structure provides enough flexibility for accurate sample placement and movement in the x-, y-, and z-directions.

A special sample container is also designed for containing biological tissues and liquids [see Fig. 2(b)]. The sample container consists of a rectangular frame of an acrylic material made from a 0.04-in (1.02 mm)-thick polycarbonate sheet. Two glass coverslips (Corning no. 1 cover glass, $\varepsilon_r = 6.6$) with dimensions of 22×50 mm^2 and 0.15-mm thick, are glued to the two sides of the frame using rubber cement glue. Liquids (e.g., water and saline) are injected inside the container through two 0.6-mm-diameter holes provided at each side. The holes are then sealed by the rubber cement glue. The exact sample container thickness can be monitored by using a z micropositioner with a resolution of $\approx$10 μm. By using an x–y micropositioner, a sample can also move to some extent across and parallel to the fixture cavities ground planes.

III. TEST-FIXTURE MODELING

A. Modeling Considerations

Test-fixture modeling has been reported previously [8], [9]. The model includes the microstrip line, apertures, glasses, TUT, and metallic housing. The absorbing boundary condition is defined to delimit the tissue boundary. A homogeneous distribution of tissue is considered in the modeling.

The modeling is performed for various frequencies from 5 to 50 GHz. Thirty-one frequency points are selected for this range. For each frequency point, the simulation time is approximately 2 min running on a SUN SPARC SOLARIS 2.5 machine. These frequency points are nonuniformly distributed in the frequency domain and selected by trial-and-error. The objective is to generate a well-behaved frequency response while assuring that any sharp variation in S_{21} magnitude would not be missed. In a similar fashion, simulations are performed for eight values of $\tan\delta$ and 12 values of ε', which are nonuniformly distributed over the range of $0.15 \leq \tan\delta \leq 2.5$ and $2.5 \leq \varepsilon' \leq 75$ (Note that ε' and ε'' refer to their relative values throughout this paper.) These values are within the expected range of biological tissues reported in the literature [5]. A total of 96 simulations each for a unique complex permittivity are performed. The simulation time requirement is approximately 6000 min or four days for the given structure. However, the simulation is performed once and the results are fitted to a proper function.

B. Fitting Simulation Data to a Mathematical Function

To cover a large number of frequencies and complex-permittivity values, it is not attractive to perform simulations for all possible cases. Alternative techniques need to be developed. It is recognized through modeling that interpolation (e.g., spline or cubic) of the tabulated data in the three-dimensional (3-D) space of f, ε', and $\tan\delta = \varepsilon''/\varepsilon'$ has some shortcomings. In fact, the complex-permittivity extraction procedure becomes very slow since a nonlinear root-search algorithm should call the interpolation routine several times before reaching a final solution. Moreover, it is observed that for the selected number of discrete f, ε', and $\tan\delta$ values used in the test-fixture modeling, the interpolation will not yield a well-behaved mathematical function for S-parameters below 25 GHz.

Therefore, it is very appealing to develop a mathematical function that allows one to predict the test fixture S-parameters in a close form. A rational function approach was already introduced by Stuchly *et al.* [13] for fitting the input admittance of a coaxial probe terminated to a medium with complex permittivity $\varepsilon = \varepsilon' - j\varepsilon''$. This approach is extended to our problem by representing its functional form in Table I, Eq. (1), where $\zeta = \sqrt{\varepsilon}$ and α_{np} and β_{mq} are the parameters of the function. These parameters are found by fitting the simulation results to this function using a least square algorithm [15] to Table I, Eq. (1). A careful study of Table I, Eq. (1) reveals that a rearrangement of

this equation with known S_{ij}, ε, and ω yields a linear equation for unknown α_{np} and β_{mq}. Such inference implies that a linear least square algorithm is a better choice than the nonlinear one suggested by Stuchly *et al.* [13], a fact that greatly reduces the computational cost.

This observation also offers a new approach. For better accuracy, instead of fitting all the data points to a unique function, as shown in Table I, Eq. (1), which turns out to not be a very accurate fitting method, an alternative method is employed. For a fixed complex permittivity, Table I, Eq. (1) reduces to a pole-zero expansion for the frequency response of a linear system, i.e., Table I, Eq. (2). For each simulated value of ε, coefficients a_n and b_m (see Table I) are found by using the linear least square fitting of the modeled S_{ij} at 31 modeling frequencies to Table I, Eq. (2). Since the measurements are usually performed at much higher number of frequency values (e.g., 301 points), S_{ij} is then calculated from Table I, Eq. (2) at each measurement frequency. Alternatively, for a fixed measurement frequency, Table I, Eq. (1) reduces to Table I, Eq. (4), which is then used to find coefficients A_p and B_q using the linear least square fitting for each measurement frequency. Therefore, for each measurement frequency, $P+Q+1$ coefficients should be saved for each S-parameter from Table I, Eq. (4). In practice, it was observed that using $\zeta = \varepsilon$ instead of $\zeta = \sqrt{\varepsilon}$ in Table I, Eq. (4) yields a slightly better fitting. Therefore, in fitting and extraction algorithms, $\zeta = \varepsilon$ is used in the procedure for that equation. The truncation used for linear least square routine is for $M = N = P = Q = 5$. The CPU run time is only approximately 1 min for evaluating A_p and B_q from Table I, Eq. (4) at 301 frequency points using a 500-MHz Pentium III processor.

A plot representing loci of S_{21} for fixed values of ε' and $\tan\delta$ is very helpful to visualize the success of this fitting procedure. Fig. 3 represents a comparison between the simulated S_{21} and S_{21} fitted to Table I, Eq. (4) at 15 GHz. These loci are, in fact, perpendicular to one another in each modeling point (o).

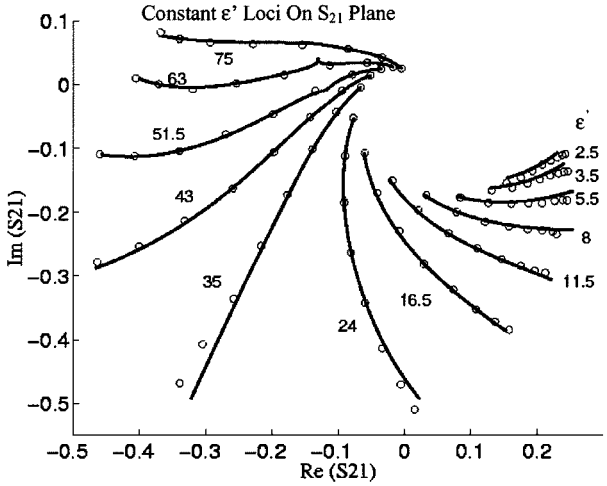

(a)

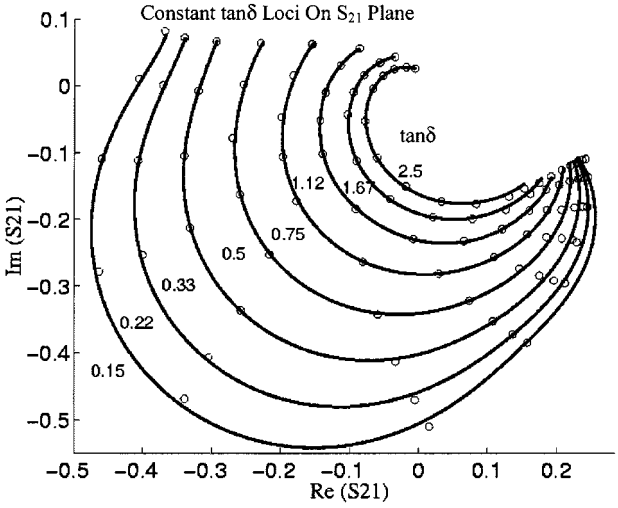

(b)

Fig. 3. Loci of fixed: (a) ε' and (b) $\tan\delta$ plotted in the S_{21}-plane at 15 GHz, obtained by the fitting method (—) to the data from the modeling (o).

C. Complex-Permittivity Extraction Procedure

The measured S_{21} deembedded to the fixture reference planes [see Fig. 1(a)] is used for the complex-permittivity extraction of TUT. Since S_{11} is very insensitive to the change of complex permittivity a small error in the measured S_{11} yields a large error in the extracted complex-permittivity values. Therefore, S_{21} is used because of its high sensitivity. With known S_{21}, ε can be found very easily; rearranging Table I, Eq. (4) for a known S_{21} (note that $\zeta = \varepsilon$), A_p, and B_q, leads to a polynomial equation of the order $\max(P, Q)$ as follows:

$$\sum_{p=0}^{P} A_p \varepsilon^p - S_{21} \sum_{q=1}^{Q} B_q \varepsilon^q - S_{21} = 0.$$

A root of this polynomial, which satisfies $\varepsilon'' > 0$ and $\varepsilon' > 1$, and is within the expected range for tissues, is selected as the physical solution.

IV. Measurement Results

An Anritsu 37397C 40-MHz–65-GHz ANA with V-type connector test ports is used for the measurement of scattering parameters. The source power level is set to -7 dBm, and 301 points are selected between 5–50 GHz (150-MHz frequency step). The ANA averaging feature is employed. Averaging is set to 30 for the calibration and ten for TUT measurements. With these selections, a typical measurement would take approximately 10 s. Measurements are performed in room temperature and any results located outside 27 ± 0.5 °C are rejected.

A. Measurement Results for Distilled Water

For high water-content tissues, the dipolar relaxation of water is the dominant factor in defining their relaxation behavior at microwave frequencies. Therefore, it is realistic to assume that the result obtained by the measurement of water can serve as a measure to identify the validity and limitation of the technique.

Measurements are performed for distilled water (lossy liquid) and methanol (low-loss liquid) to observe the change of S-parameters with displacing the aperture with respect to the sample container wall. The measurement results prove that, for frequencies above approximately 15 GHz, as long as the aperture is located on the sample and 2–3 mm away from walls of the

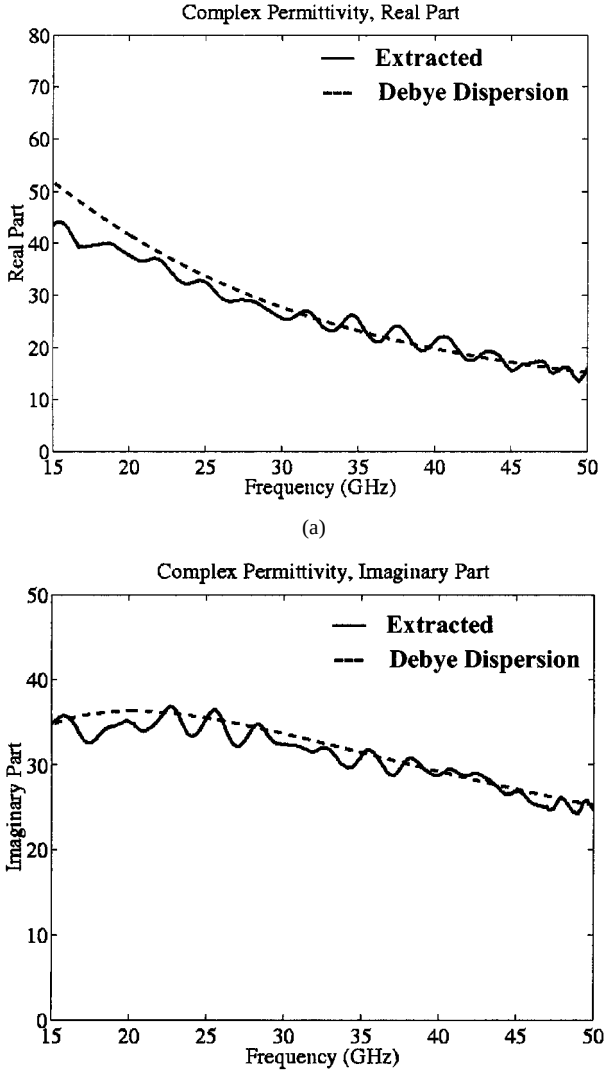

Fig. 4. Extracted (—) and Debye model [16] (- - -) results of the complex permittivity ε ($\varepsilon = \varepsilon' - j\varepsilon''$) for distilled water at 27 °C as a function of frequency. (a) Real part (ε'). (b) Imaginary part (ε'').

sample container [see Fig. 2(b)], the measured S-parameters are not sensitive to the location of the aperture over the sample container.

The extracted ε' and ε'' for distilled water are given in Fig. 4 for frequencies of 15–50 GHz. A single-term Debye relaxation is generally accepted for water dispersion at microwave frequencies [16]. At 27 °C, the relaxation time (τ) and static permittivity (ε_s) are 7.7 ps and 77.6, respectively. The optical permittivity (ε_∞) is selected as 4.9 [16]. The real and imaginary parts of the complex permittivity obtained by this model are also depicted for the comparison with the extracted results in Fig. 4. The agreement is very good above 20 GHz. The ripple-like behavior is as a result of the lack of repeatability in performance of the coaxial-to-microstrip launchers. A sensitivity analysis, with the sensitivity of S_{21} with respect to complex permittivity defined as $|\varepsilon/S_{21}|(\partial S_{21}/\partial\varepsilon)$ [13], reveals that the S_{21} sensitivity for water increases monotonically from 3 to 7 dB for the frequency range of 15–50 GHz. This fact is the main reason for higher errors at lower frequencies.

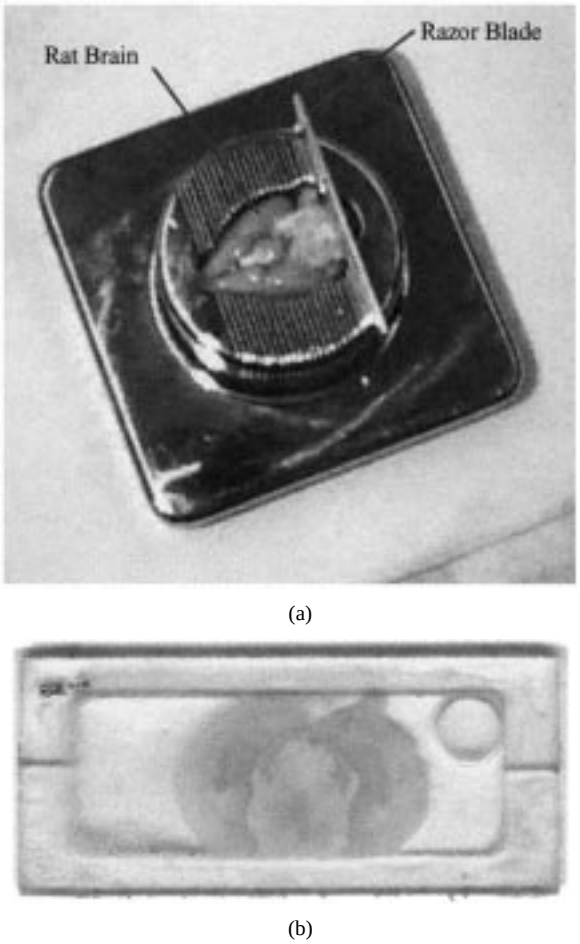

Fig. 5. (a) Rat brain is sliced on a rodent-brain matrix. (b) Photograph of a typical slice of rat brain inside a sample container filled with saline.

B. Tissue Preparation

Fresh rat brains from male Sprague Dawley rats (∼400 g) are directly removed after euthanasia and placed in a phosphate buffer 0.1 M pH 7.4 until ready to be cut. The brains were placed on a rodent brain matrix and sliced in a coronal orientation at intervals of 2 mm (i.e., slice thickness before placement in the sample container) with a razor blade [see Fig. 5(a)]. To maintain these slices fresh, they were stored in dry ice at −70 °C. The samples reach the room temperature within a few minutes after being taken out of the container. To enclose the tissue, it is placed inside the sample container frame already glued to a cover glass at the bottom. Another cover glass is then glued on top of the sample container frame, and the tissue is completely enclosed [see Fig. 5(b)]. To prevent any artifact in measurements due to air (with permittivity significantly different from the sample itself), the saline 0.9% was injected through the sample container holes into the container. This also prevents the tissue from dehydration.

Brain is approximated as an incompressible material. Therefore, by fitting the 2-mm-thick sample inside the 1-mm-thick container [see Fig. 2(a)], the tissue expands laterally. The expansion factor is in the order of 1.4 until it gets the same thickness of the frame. This technique has been observed to provide a perfect glass tissue interfacing, free from any air bubble or saline. Furthermore, this expansion increases the homogeneity of the

sample area under the aperture. Air bubbles may appear overtime in saline medium due to an imperfect water seal. As long as these air bubbles are kept at least a few millimeters away from the aperture, their impact on the measurements is observed to be insignificant.

S-parameter measurements were performed for the cerebral cortex in the front brain and pons in the back of the brain as grey and white matters, respectively. A relatively high proportion of nerve-cell nuclei exists in grey matter, whereas white matter consists mainly of axons. The color of the white matter is due to the lipid–protein sheath around these axons.

Five measurements for grey matter were performed from three slices, and six measurements for white matter were taken from a set of three different slices. Once a slice was embedded in the container and the container was filled with saline (1–2 min), its measurement took approximately 5 min, which varied depending on the number of measurements per slice. The time spent was primarily due to the accurate aperture positioning. Any measurement that was associated with water leakage from the sample container was also rejected.

C. Correction for the Lack of Repeatability of Launchers

Small ripple-like behaviors are observed for the extracted ε' and ε''. These ripples are due to the lack of performance repeatability of coaxial-to-microstrip launchers employed in TRL calibration standards and the test fixture. However, these ripples are similar for measurements of tissue and water since the test fixture launchers are the same for all TUT measurements. A correction technique is successfully employed to remove these ripples from the tissue measurement. This technique calculates the ratio of S_{21} values between the simulated (shown as ... in Fig. 6) and measured (shown as .-.-. in Fig. 6) results of distilled water. This ratio is applied as a correction factor to the measured tissue S_{21}, as will now be explained. Note that the correction factor corresponds to the difference in magnitude (in decibels) and phase values between the two cases.

D. Extraction of the Complex Permittivity of Brain Matter

The correction factor that was derived above is multiplied to the measured S_{21} for the tissue. The result of this correction applied to the measured S_{21} (shown as - - - in Fig. 6) for grey matter is also depicted (shown as — in Fig. 6). Note that an analytical proof has verified such an intuitive correction approach to remove the ripples from tissue measurement, as indicated in Fig. 6. This proof is not being reported here due to space limitations. To further emphasize its significance, it should be mentioned that the result of this simple correction is better than the one obtained by employing a generalized two-port calibration studied by the authors [9]. In that approach, calibration standards are chosen from the known materials embedded in the test fixture. Therefore, the launchers would remain the same for calibration and tissue measurements.

The extracted complex-permittivity values for white and grey matters obtained after applying this correction are shown in Figs. 7 and 8, respectively. The results are compared to the results of a four-term Cole–Cole dispersion relation provided by Gabriel *et al.* (the relation is obtained based on the measured

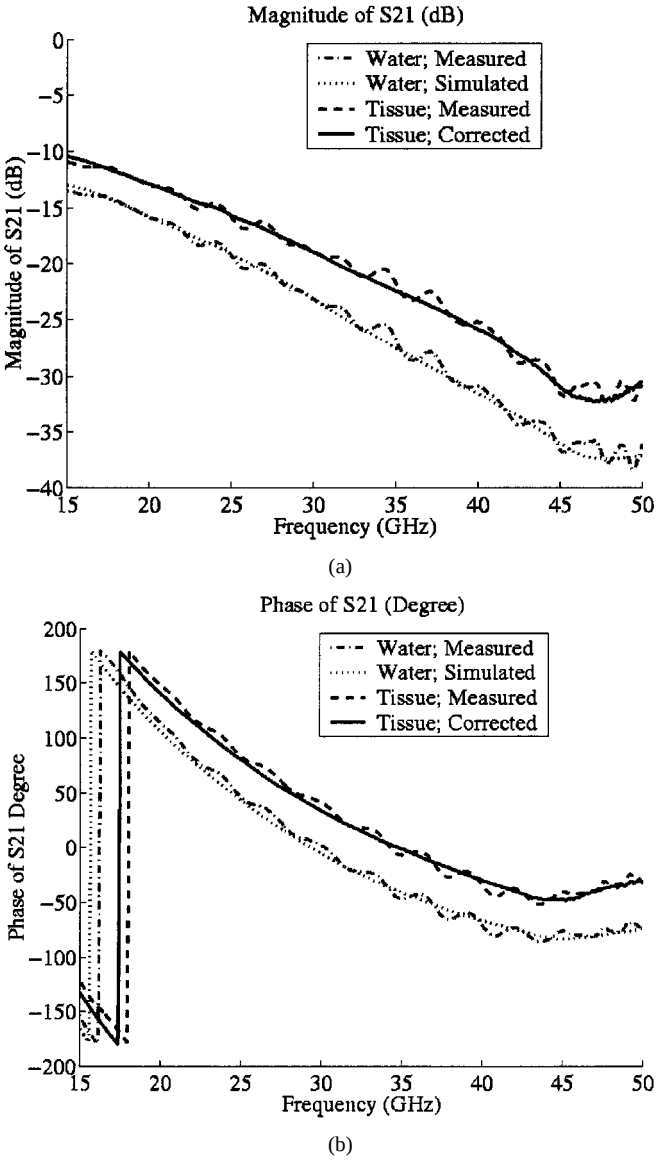

Fig. 6. Measured S_{21} of distilled water (-.-.) and grey matter (- - -) from TRL calibration, simulated S_{21} for water (. . .), and corrected S_{21} of grey matter (—). (a) Magnitude. (b) Phase.

data below 20 GHz) [17], and a newer two-term Cole–Cole dispersion relation for rat brain at 24 °C for grey matter and 25 °C for white matter given by Bao *et al.* (the relation is obtained from measured data below 26.5 GHz) [18]. These results are also compared to the measurement results for rabbit by Steel and Sheppard [19] at 35 GHz, by applying a linear interpolation for 27 °C from their tabulated results given at two different temperatures (i.e., 20 °C and 37 °C). The results suggest that the extracted complex-permittivity values for grey and white matters match better to the model provided by Bao *et al.* [18] and Gabriel *et al.* [17], respectively. Nonetheless, a further refinement of the published Cole–Cole models seems necessary as the extracted results are matched with the published ones at 35 GHz [19].

E. Fitting the Complex Permittivity to Cole–Cole Relation

The extracted results show Cole–Cole-like dispersion characteristics, with a characteristic frequency (peak of absorption)

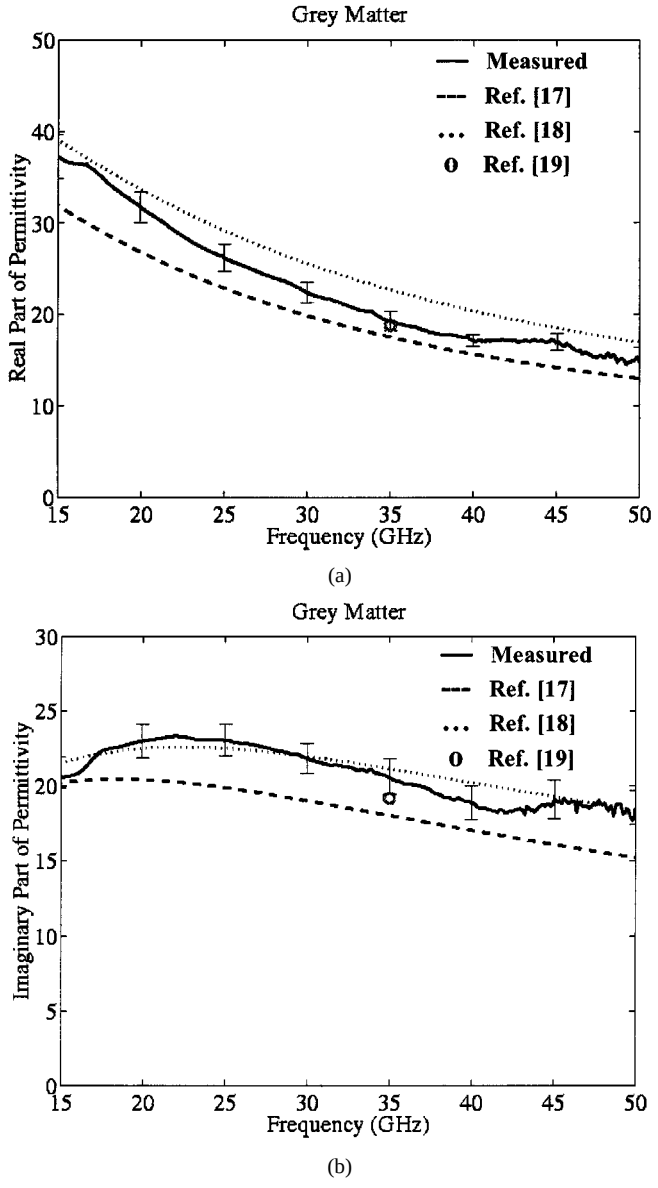

Fig. 7. Extracted complex permittivity ε ($\varepsilon = \varepsilon' - j\varepsilon''$) for grey matter at 27 °C as a function of frequency compared with the literature. (a) Real part (ε'). (b) Imaginary part (ε'').

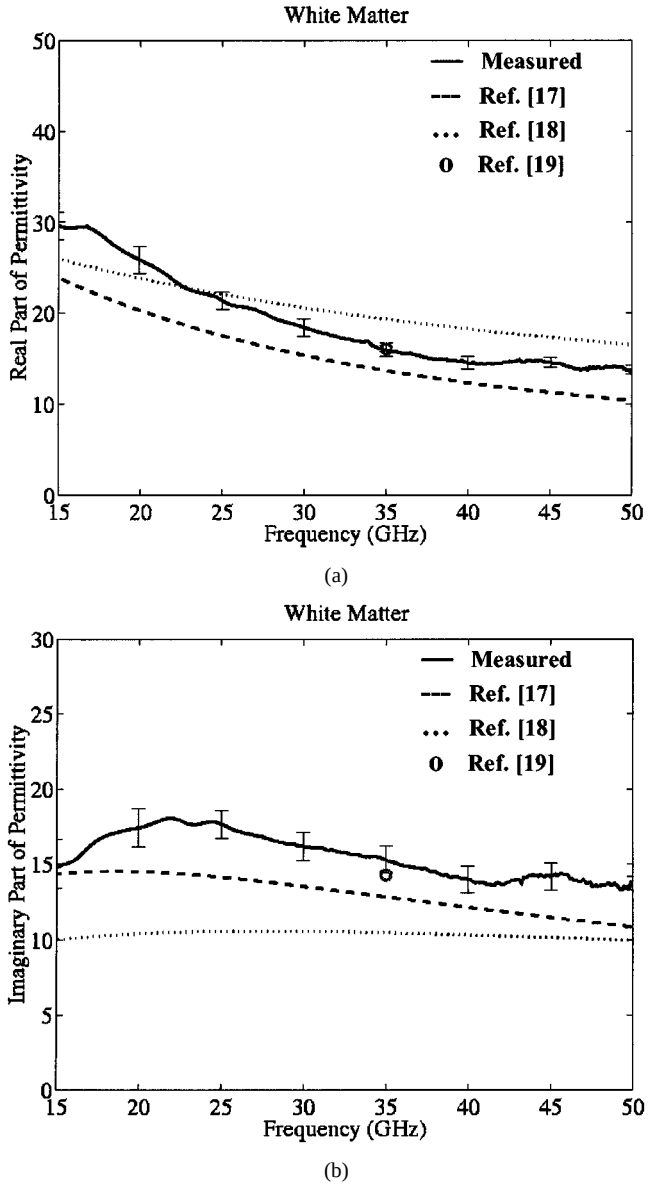

Fig. 8. Extracted complex permittivity ε ($\varepsilon = \varepsilon' - j\varepsilon''$) for white matter at 27 °C as a function of frequency compared with the literature. (a) Real part (ε'). (b) Imaginary part (ε'').

around 22 GHz for both grey and white matters. Using a nonlinear least square fitting method [15], the results of Figs. 7 and 8 are fitted to a single-term Cole–Cole relation for γ dispersion

$$\varepsilon = \varepsilon_\infty + \frac{(\varepsilon_s - \varepsilon_\infty)}{1 + (j\omega\tau)^{1-\alpha}} + \frac{\sigma}{j\omega\varepsilon_0}.$$

To account for the existing data at lower frequencies, published permittivity results above 1 GHz for white and grey matters [20], [21] are also included in the fitting procedure. Table II provides the Cole–Cole parameters obtained by this fitting, where a further refinement to the published model parameters [17], [18] is made.

F. Measurement Uncertainty

The uncertainty in ε' and ε'' resulted from S_{21} error are associated with a number of sources, which include: 1) sample container thickness tolerance; 2) fitting error; and 3) error in the reference water complex permittivity due to its temperature uncertainty. The measurement's systematic errors are already reduced to a level sufficiently below the other errors by TRL calibration and water-based correction methods that were explained before. Numerical modeling error is also reduced by careful study of the fixture response for known two-port networks formed by removing TUT (i.e., replacing it with an air gap) and changing the separation between the apertures.

The uncertainties are referred to as $\delta\varepsilon_i'$ and $\delta\varepsilon_i''$ (for real and imaginary parts, respectively), where i is the index for identifying various independent contributors. Then, the total uncertainties are

$$\delta\varepsilon'_{\text{tot}} = \sqrt{\sum_i (\delta\varepsilon_i')^2} \quad \delta\varepsilon''_{\text{tot}} = \sqrt{\sum_i (\delta\varepsilon_i'')^2}.$$

Our approach is to evaluate the uncertainties in S_{21}, i.e., $\delta S_{21,i}$ through modeling and simulation. Once they are known, the cor-

TABLE II
COLE–COLE PARAMETERS OF BRAIN WHITE AND GRAY MATTERS FOR γ DISPERSION ABOVE 1 GHz. MEASUREMENT RESULTS OF THIS STUDY ABOVE 15 GHz AT 27 °C AND THE PUBLISHED RESULTS OF THE LITERATURE [20], [21] ABOVE 1 GHz WERE INCLUDED TO OBTAIN THESE PARAMETERS

	τ (ps)	ε_s	ε_∞	σ (S/m)	α
Grey Matter	6.75	49.5	5.8	0.96	0
White Matter	6.34	37.3	5.3	0.79	0

TABLE III
MEASUREMENT UNCERTAINTY, $\delta\varepsilon_i'$ AND $\delta\varepsilon_i''$, FROM VARIOUS SOURCES ($i = 1$, FITTING ERROR, 2, TISSUE THICKNESS, 3, REFERENCE TEMPERATURE, AND 4, APERTURE PLACEMENT ON TISSUE), THE TOTAL UNCERTAINTIES, $\delta\varepsilon_{\rm tot}'$ AND $\delta\varepsilon_{\rm tot}''$, AND THE TOTAL RELATIVE UNCERTAINTIES, $\delta\varepsilon_{\rm tot}'/\varepsilon'$ AND $\delta\varepsilon_{\rm tot}''/\varepsilon''$, OBTAINED FOR WHITE AND GREY MATTERS AT 30 GHz

	$\delta\varepsilon'_1$	$\delta\varepsilon''_1$	$\delta\varepsilon'_2$	$\delta\varepsilon''_2$	$\delta\varepsilon'_3$	$\delta\varepsilon''_3$	$\delta\varepsilon'_4$	$\delta\varepsilon''_4$	$\delta\varepsilon'_{\rm tot}$	$\delta\varepsilon''_{\rm tot}$	$\delta\varepsilon'_{\rm tot}/\varepsilon'$	$\delta\varepsilon''_{\rm tot}/\varepsilon''$
Grey	0.7	0.1	0.1	0.2	0.2	0.2	1.2	1.0	1.4	1.1	0.06	0.05
White	0.6	0.1	0.1	0.2	0.1	0.2	1.0	0.9	1.1	1.0	0.06	0.06

responding uncertainty in the complex permittivity can be estimated through the relation

$$\delta\varepsilon_i = \delta\varepsilon_i' - j\delta\varepsilon_i'' = \frac{\delta S_{21,i}}{(\partial S_{21}/\partial\varepsilon)}$$

where the denominator can be easily obtained using Table I, Eq. (4).

The first source of error is the uncertainty in fitting of S_{21} (i.e., $\delta S_{21,1}$) that is evaluated at a set of frequency and complex-permittivity values used in the numerical modeling that is closest to the one that the measurement uncertainty is being estimated. Simulations were also performed to evaluate $\delta S_{21,2}$ due to the sample container's thickness variation that is estimated as ± 10 μm, derived by measurement of various sample containers. In addition, the change in the reference water temperature as ± 0.5 °C will result in $\delta S_{21,3}$. On the other hand, there is some uncertainty due to the placement of aperture on top of a white- or grey-tissue region, which might not be exactly of the same texture, composition, or placement for all measurements (i.e., placement uncertainty, $\delta S_{21,4}$).

Table III lists the result of various uncertainties and the total uncertainties obtained from the above uncertainty equations for measurement at 30 GHz. The placement uncertainty ($\delta\varepsilon_4$) is obtained by repetitive tissue measurements and taking the standard deviation of the extracted results. This source of uncertainty is clearly the dominant factor. The same analysis is repeated for selected frequencies from 15 to 50 GHz. The results of this analysis have been already shown as error bars in Figs. 7 and 8. The uncertainty for both real and imaginary parts of the complex permittivity varies from 4% to 8% for the entire range, except the real part above 45 GHz, where error exceeds 10%.

V. CONCLUSIONS

A two-port microstrip test fixture has been designed and fabricated for the extraction of complex permittivity of biological tissues. In particular, an extraction technique is developed for the complex-permittivity measurements of brain grey and white matters up to 50 GHz. Since the fixture S-parameters are numerically modeled using the finite-element method, a closed-form analytical solution does not exist. However, a fitting procedure is introduced to fit the data obtained from the modeling to a rational function using the linear least square approach. The fitting procedure reported here is unique since it is computationally more efficient than previously proposed ones [12], [13] and, in addition, is more accurate. Furthermore, a set of rational function parameters is obtained for each measurement frequency and is used for extraction in that frequency.

The complex permittivity of brain white and grey matters is extracted from measurements of slices of rat brain. A technique is introduced to remove the residual errors due to the lack of performance repeatability of the coaxial-to-microstrip launchers of the TRL calibration standards. This correction technique utilizes the comparison of measured and simulated S_{21} of distilled water (as a reference). The extracted $\varepsilon' - j\varepsilon''$ for brain matters are compared to the existing Cole–Cole models and previously reported brain data at 35 GHz. Finally, the measured results are fitted to single term Cole–Cole relations to represent the γ dispersion of white and grey matters obtained by direct measurements up to 50 GHz. The uncertainty of the final extraction result is less than 8% up to 45 GHz and primarily due to the variability within the tissue where the apertures might face regions with slightly different compositions. Nonetheless, the extracted Cole–Cole parameters are significant improvements over the published parameters that are based on the one-port measurement up to 26.5 GHz.

ACKNOWLEDGMENT

The authors thank J. Cacciola, Anritsu Company, Pine Brook, NJ, and D. Rangel, Anritsu Company, for providing the 37397C ANA. The authors greatly appreciate the assistance of W. Janton, Sarnoff Corporation, Princeton, NJ, for fabrication of the test fixture assembly and L. Bertrand, MCP Hahnemann University, Philadelphia, PA, for preparation of rat brain samples.

REFERENCES

[1] *IEEE Trans. Microwave Theory Tech. (Special Issue)*, vol. 48, Nov. 2000.
[2] A. Rosen and H. Rosen, Eds., *New Frontiers in Medical Device Technologies.* New York: Wiley, 1995.

[3] O. P. Gandhi, G. Lazzi, and C. M. Furse, "Electromagnetic absorption in the human head and neck for mobile telephones at 835 and 1900 MHz," *IEEE Trans. Microwave Theory Tech.*, vol. 44, pp. 1884–1897, Oct. 1996.
[4] Y. Nikawa, N. Hoshi, K. Kawai, and S. Ebisu, "Study on dental diagnosis and treatment using millimeter waves," *IEEE Trans. Microwave Theory Tech.*, vol. 48, pp. 1783–1788, Nov. 2000.
[5] C. Gabriel, S. Gabriel, and E. Corthout, "The dielectric properties of biological tissues: I. Literature review," *Phys. Med. Biol.*, vol. 41, pp. 2231–2249, 1996.
[6] F. Duhamel, I. Huynen, and A. Vander Vorst, "Measurements of complex permittivity of biological and organic liquids up to 110 GHz," in *IEEE MTT-S Int. Microwave Symp. Dig.*, vol. 1, New York, NY, 1997, pp. 107–110.
[7] E. C. Burdette, F. L. Cain, and J. Seals, "*In vivo* probe measurement technique for determining dielectric properties at VHF through microwave frequencies," *IEEE Trans. Microwave Theory Tech.*, vol. MTT-28, pp. 414–424, Apr. 1980.
[8] M. R. Tofighi and A. S. Daryoush, "Characterization of biological tissues up to millimeter wave: Test fixture design," in *IEEE MTT-S Int. Microwave Symp. Dig.*, vol. 2, June 2000, pp. 1041–1044.
[9] M. R. Tofighi, "Design and implementation of a two-port microstrip test fixture for complex permittivity characterization and near field imaging of biological materials up to 50 GHz," Ph.D. dissertation, Dept. Elect. Eng., Drexel Univ., Philadelphia, PA, 2001.
[10] G. F. Eagen and C. A. Hoer, "Thru-reflect-line: An improved technique for calibrating the dual six-port automatic network analyzer," *IEEE Trans. Microwave Theory Tech.*, vol. MTT-27, pp. 987–993, Dec. 1979.
[11] J. C. Lin, "Microwave properties of fresh mammalian brain tissues at body temperature," *IEEE Trans. Bio-Med. Eng.*, vol. BME-22, pp. 74–76, Jan. 1975.
[12] J. Abdulnour, C. Akyel, and K. Wu, "A generic approach for permittivity of dielectric materials using a discontinuity in a rectangular waveguide or a microstrip line," *IEEE Trans. Microwave Theory Tech.*, vol. 43, pp. 1060–1066, May 1995.
[13] S. S. Stuchly, C. L. Sibbald, and J. M. Anderson, "A new admittance model for open-ended waveguides," *IEEE Trans. Microwave Theory Tech.*, vol. 42, pp. 192–198, Feb. 1994.
[14] H. P. Schwan and K. R. Foster, "RF-field interactions with biological systems: Electrical properties and biophysical mechanism," *Proc. IEEE*, vol. 68, pp. 104–113, Jan. 1980.
[15] W. H. Press, *Numerical Recipes in C: The Art of Scientific Computing*. New York: Cambridge Univ. Press, 1992.
[16] A. Stogryn, "Equations for calculating the dielectric constant of saline water," *IEEE Trans. Microwave Theory Tech.*, vol. MTT-19, pp. 733–736, Aug. 1971.
[17] S. Gabriel, R. W. Lau, and C. Gabriel, "The dielectric properties of biological tissues: III. Parametric models for the dielectric spectrum of tissues," *Phys. Med. Biol.*, vol. 41, pp. 2271–2293, 1996.
[18] J. Bao, S. Lu, and w. D. Hurt, "Complex dielectric measurements and analysis of brain tissues in the radio and microwave frequencies," *IEEE Trans. Microwave Theory Tech.*, vol. 45, pp. 1730–1740, Oct. 1997.
[19] M. C. Steel and R. J. Sheppard, "The dielectric properties of rabbit tissue, pure water and various liquids suitable for tissue phantoms at 35 GHz," *Phys. Med. Biol.*, vol. 33, pp. 467–472, 1988.
[20] M. A. Stuchly and S. S. Stuchly, "Dielectric properties of biological substances-tabulated," *J. Microwave Power*, vol. 15, no. 1, pp. 19–26, 1980.
[21] F. A. Duck, *Physical Properties of Tissue: A Comprehensive Reference Book*. London, U.K.: Academic, 1990.

Mohammad-Reza Tofighi (S'98–M'00) received the B.S.E.E. degree from the Sharif University of Technology, Tehran, Iran, in 1989, the M.S.E.E. degree from the Iran University of Science and Technology, Tehran, Iran, in 1993, and the Ph.D. degree in electrical engineering from Drexel University, Philadelphia, PA in 2001.

Since April 2001, he has been a Post-Doctoral Research Associate with the Department of Electrical and Computer Engineering, Drexel University, where he has been involved in research in the interaction of electromagnetic field with biological materials at microwave and millimeter-wave frequencies, and development of microwave and millimeter-wave measurement test fixtures and circuits.

Afshin S. Daryoush (S'84–M'86–SM'91–F'99) received the Ph.D. degree in electrical engineering from Drexel University, Philadelphia, PA in 1986.

Upon graduation, he joined the faculty of Drexel University, as DuPont Assistant Professor of Electrical and Computer Engineering. He became an Associate Professor and Associate Director of the Center for Microwave/Lightwave Engineering in 1990 and a Full Professor in 1998. He was a Summer Faculty Fellow with the NASA–Lewis Research Center, Cleveland, OH. In the summers of 1989 and 1990, he was with the Naval Air Development Center, Warminster, PA. During the 1996–1997 academic year, he was on sabbatical leave from Drexel University, and was a Visiting Scholar with the NTT Wireless Systems Laboratories, Yokosuka, Japan. He holds four U.S. patents, one of which is now licensed for commercialization. He has developed and taught a variety of undergraduate and graduate courses in electromagnetic fields, microwave and photonic devices, RF circuits, and antennas. He has also conducted research in microwave photonics resulting in publication of over 200 technical papers. He has served as guest editor for *The Journal of Franklin Institute* and *Microwave and Lightwave Technology Letters*.

Prof. Daryoush is a member of Sigma Xi, and served as president of the Drexel University Chapter in 1999. He has also served as the IEEE Philadelphia Joint Chapter of the Antennas and Propagation (AP)/Microwave Theory and Techniques (MTT) societies in various capacities, such as vice chair, chair, and ex-officio from 1989 to 1995. As the chapter officer, he co-organized the annual Benjamin Franklin Symposium and is one of the organizers of the 2003 IEEE Microwave Theory and Techniques Society (IEEE MTT-S) International Microwave Symposium, Philadelphia, PA. He is a member of the IEEE MTT-3 Technical Committee on Lightwave Engineering. He has also served as member of the Technical Program Committee of the IEEE MTT-S, IEEE AP-S, and IEEE Lasers and Electro-Optics Society (IEEE LEOS)-sponsored international meetings, and has organized and lectured in a number of IEEE sponsored workshops. He was the recipient of the 2000 University Graduate Teaching Award and the 16th European Microwave Conference Microwave Prize. He has also been the recipient of the 1986 and 1994 Best Presentation Awards presented at the IEEE MTT-S International Microwave Symposia.